

Article

Estimation of the Restored Forest Spatial Structure in Semi-Arid Mine Dumps Using Worldview-2 Imagery

Xiaoxiao Zhu ¹, Yongli Zhou ², Yongjun Yang ^{1,3}, Huping Hou ^{1,3,*}, Shaoliang Zhang ^{1,3} 
and Run Liu ¹

¹ School of Environment Science and Spatial Informatics, China University of Mining and Technology, Xuzhou 221008, China; xxzhu@cumt.edu.cn (X.Z.); y.yang@cumt.edu.cn (Y.Y.); slzhang@cumt.edu.cn (S.Z.); lrstyle@126.com (R.L.)

² Shenhua Zhungeer Energy Company Limited, Ordos 010399, China; zhouyongli_1981@163.com

³ Ministry of Education Engineering Research Centre or Mine Ecological Restoration, Xuzhou 221008, China

* Correspondence: hphou@163.com; Tel.: +86-138-5214-4183

Received: 8 April 2020; Accepted: 19 June 2020; Published: 23 June 2020



Abstract: Forest monitoring is critical to the management and successful evaluation of ecological restoration in mined areas. However, in the past, available monitoring has mainly focused on traditional parameters and lacked estimation of the spatial structural parameters (SSPs) of forests. The SSPs are important indicators of forest health and resilience. The purpose of this study was to assess the feasibility of estimating the SSPs of restored forest in semi-arid mine dumps using Worldview-2 imagery. We used the random forest to extract the dominant feature factor subset; then, a regression model and mind evolutionary algorithm-back propagation (MEA-BP) neural network model were established to estimate the forest SSP. The results show that the textural features found using 3×3 window have a relatively high importance score in the random forest model. This indicates that the 3×3 texture factors have a relatively strong ability to explain the restored forest SSPs when compared with spectral factors. The optimal regression model has an R^2 of 0.6174 and an MSRE of 0.1001. The optimal MEA-BP neural network model has an R^2 of 0.6975 and an MSRE of 0.0906, which shows that the MEA-BP neural network has greater accuracy than the regression model. The estimation shows that the tree–shrub–grass mode with an average of 0.7351 has the highest SSP, irrespective of the restoration age. In addition, the SSP of each forest configuration type increases with the increase in restoration age except for the single grass configuration. The increase range of SSP across all modes was 0.0047–0.1471 after more than ten years of restoration. In conclusion, the spatial structure of a mixed forest mode is relatively complex. Application cases show that Worldview-2 imagery and the MEA-BP neural network method can support the effective evaluation of the spatial structure of restored forest in semi-arid mine dumps.

Keywords: forest spatial structure; Worldview-2; MEA-BP neural network; semi-arid mine dumps; ecological restoration

1. Introduction

The species planted for reforestation in mine dumps of semi-arid areas have been planted based on local conditions such as environmental suitability, after which natural succession occurs. This gives forests in these areas the characteristics of having a simple spatial structure and weak heterogeneity, which is different from natural forests. The spatial structural parameters (SSPs) of these restored forests in semi-arid mine dumps are important indicators used for evaluating the quality of ecological restoration at post-mining sites and are of great significance for the monitoring and management of

ecological restoration projects. The estimation of forest SSPs is important when testing the effectiveness of forest restoration measures and reducing the risk of future degradation of restored forest land.

Currently, research on the spatial structure of forests is lacking related to the evaluation of ecological restoration success in mine areas [1]. The rapid and accurate estimation of large-scale forest structural parameters is an important basis for formulating sustainable forest management measures [2], especially plantation management [3]. It has huge application potential in forest resource management planning [4]. Existing studies explored the stability of forest structure [5] and evaluated the economic and ecological benefits of forestry [6] through forest structure parameters. Two main methods currently exist for obtaining the parameters of the forest spatial structure. Traditional methods used to acquire information on forest spatial structure parameters usually rely on ecological field surveys, and the common method of investigating forests is per wooden locator. The survey parameters include: number of trees, basal area, stem volume [7], location [8], height [9], base perimeter, canopy size, and so on [10]. Ecological field surveys are expensive, inefficient, and make full coverage of the study site difficult to achieve. At present, high-resolution remote sensing technology has the advantages of producing results rapidly, having a wide range, low cost, and high accuracy to provide rich forest spectral and textural information [11–13]. By transforming the spectra [14,15] and using spatial analysis [16], a great amount of forest information can be mined from this data source. However, few studies have investigated the ability of Worldview in inverting the spatial structure of forests.

Remote sensing has been widely introduced into the study of forest parameters. Generally, forest parameters such as vegetation coverage [1,17], vegetation index [18–21], and leaf area index [22] are obtained using medium-resolution satellite images, such as imagery from Landsat [23,24] and Sentinel-2 satellites [25]. Researchers have extracted the Normalized Difference Vegetation Index (NDVI) [26], Soil Adjusted Vegetation Index (SAVI) [27], leaf area index [28], chlorophyll [29], Net Primary Production [30], and forest water content [31] from remote sensing images. These parameters become connections between observed forest parameters and soil structure, ecosystems [32–34], climate environment [35], and so on, which are employed for evaluating the success of ecological restoration. However, medium-resolution satellite imagery provides only a limited amount of information, and fine structures are difficult to extract. This limits the quantitative extraction of forest parameters and the evaluation of the success of ecological restoration. Further research has proven that high spatial resolution images provide more detailed forest information [36–38], which can greatly improve the accuracy of estimation results.

The purpose of this paper is to use a readily available multispectral sensor (Worldview-2) to estimate the restored forest spatial structure parameters in semi-arid mine dumps, especially for: (1) determining the dominant feature factor subset of forest SSP; (2) establishing a forest SSP estimation model based on field sampling data; and (3) discussing the variability of spatial structure for different forest allocation techniques during different restoration years.

2. Materials and Methods

2.1. Study Area

The study area is located in the Heidaigou open-pit coal mine of the Shenhua Zhungeer Energy Co. Ltd., Inner Mongolia, China, at 39°38′–52′ N, 110°06′–111°24′ E and about 125 km northeast of Ordos (Figure 1). The terrain is mainly hilly, with an elevation of 1025–1302 m. The semi-arid climate of the middle temperate zone has an average annual precipitation and temperature of about 350–450 mm and 7.2 °C, respectively.

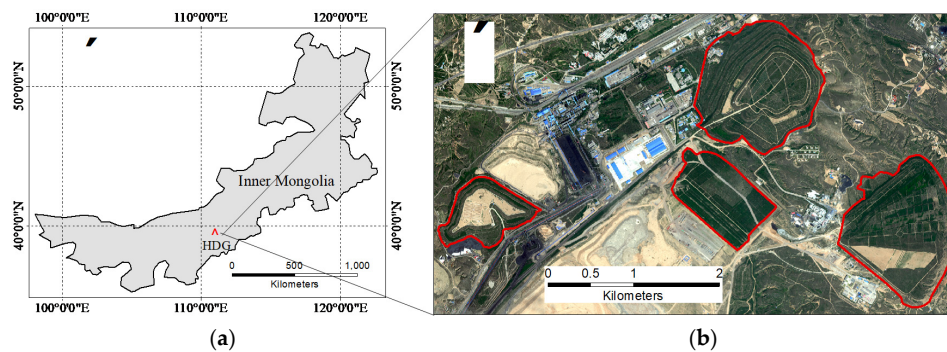


Figure 1. (a) Map of Inner Mongolia, China showing the location of the study area; and (b) Worldview-2 image of the study area acquired in 2018, showing the layout of the four mine dumps.

Since the construction and production of Heidaigou Coal Mine started in 1990, the surface forest ecosystem has been severely damaged due to the large-scale excavation of infrastructure and mine production projects. Forests promote soil structure restoration and fertility, while also providing protection from soil and water erosion. Therefore, the plantation and growth of forests is the primary aspect of ecological restoration. Land restoration work started in 1992. Six mine dumps exist in the mining area. Here, four of them were selected for research. The dump site had a steep slope and a thin soil layer, which was very unfavorable to water retention and plant seed settlement. Therefore, the dump site needed to be leveled and covered before planting. During vegetation selection, native plants and pioneer plants that can naturally become established in industrial wastelands were preferred. In dumps, slopes were mainly planted with a tree–shrub–grass combination of plants to prevent soil erosion and the terraces where planted with legumes and sea buckthorn to provide soil maturation. The row spacing of trees was about 2–4 m, and shrubs was about 1.5–2 m. The main types of forest in the north dump are *Hippophae rhamnoides*, *Caragana korshinskii*, *Pinus tabulaeformis*, and *Populus euphratica*; the forest reached full coverage of the landscape in 2010. The east dump was mainly planted with *Glycyrrhiza uralensis*, *Leymus secalinus*, and *P. euphratica*; the forest coverage reached 80% in 2008. The forest of the west dump site is populated by *Calamagrostis epigejos* and *Populus spp.*, which covers the surrounding area. The forest in the inner dump is covered by *C. epigejos* and *forb meadow*; the coverage peaked in 2010. Native remnant forest species included *Stipa bungeana*, *Thymus serpyllum*, and *Heteropappus altaicus*, which were scattered with a coverage of <30%.

2.2. Forest Spatial Structure

The organization of forest structure can reflect the species of forest communities and their interrelationships. It can also represent the complexity and diversity of forest structures. Numerous studies have shown that the organizational structure of forest communities includes not only species diversity, but also the diversity of spatial structure, such as differences in tree diameter at breast height (DBH) and height. An ideal forest community structure can be simply described as stratified, uneven-aged, and mixed. The higher the structural diversity becomes, the more stable the stand structure will be [39].

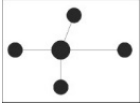
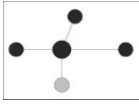
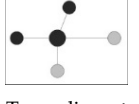
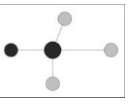
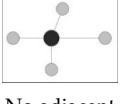
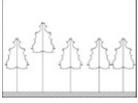
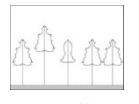
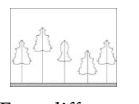
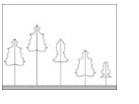
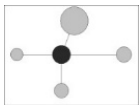
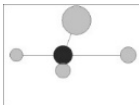
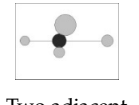
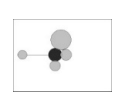
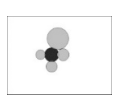
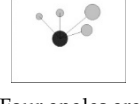
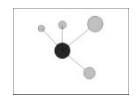
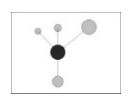
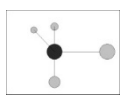
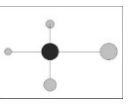
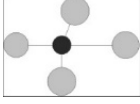
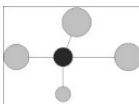
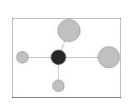
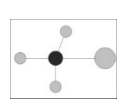
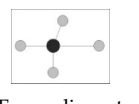
2.2.1. Definition of Spatial Structure Units

This study focused on the spatial matching relationship of the measured objects. We set up a survey unit of the spatial structure of the forest community on the quadrat scale to extract the information of the SSPs of forest land. The specific principle was the comparison of feature measurement between any tree object in the unit and the four nearest trees. At the level of structural data measurement, the SSPs of the forest community were constructed to be characterized by their horizontal and vertical structural feature.

2.2.2. Construction of Index System

We constructed six indices to characterize the spatial structure of forest (Table 1): tree species mixture (M), differentiation of forest layer (D), density (C), angle (W), DBH size ratio (U), and height size ratio (H) indices.

Table 1. Forest spatial structure index system.

Index	0	0.25	0.5	0.75	1
M	 Four adjacent trees are same species as the reference tree (no mixing)	 Three adjacent trees are same species as the reference tree (weak mixing)	 Two adjacent trees are same species as the reference tree (medium mixing)	 One adjacent tree is same species as the reference tree (strong mixing)	 No adjacent trees are same species as the reference tree (extreme mixing)
D	 Five adjacent trees have the same properties (no difference)	 Two different properties (light difference)	 Three different properties (medium difference)	 Four different properties (strong difference)	 Five different properties (major difference)
C	 No adjacent trees overlap with the reference crown (very sparse)	 One adjacent tree overlaps with the reference crown (relative sparse)	 Two adjacent trees overlap with the reference crown (medium sparse)	 Three adjacent trees overlap with the reference crown (relative dense)	 Four adjacent trees overlap with the reference crown (very dense)
W	 Four angles are less than the standard angle α_0 (Very uneven distribution)	 Three angles are less than the standard angle α_0 (uneven distribution)	 Two angles are less than the standard angle α_0 (random distribution)	 One angle is less than the standard angle α_0 (even distribution)	 No angles are less than the standard angle α_0 (Very even distribution)
U/H	 No adjacent trees are smaller than reference trees (absolute disadvantage)	 One adjacent tree is smaller than reference trees (disadvantage)	 Two adjacent trees are smaller than reference trees (moderate)	 Three adjacent trees are smaller than reference trees (Sub-advantage)	 Four adjacent trees are smaller than reference trees (absolute advantage)

Tree species mixture (M) was calculated as M_i using Equation (1):

$$M_i = \frac{1}{4} \sum_{j=1}^4 W_{ij} W_{ij} = \begin{cases} 1, & \text{different tree species} \\ 0, & \text{same tree species} \end{cases} \quad (1)$$

where W_{ij} is a discrete variable.

This index (M_i) reflects the complexity of tree species configuration in the structural unit and is defined by the proportion of the number of tree species differing from the reference number.

Differentiation of forest layer (D): D_i was calculated using Equation (2):

$$D_i = \frac{N_i - 1}{4} \quad (2)$$

where N_i is the number of different attribute types in the spatial structural unit formed by the i_{th} reference tree, with values ranging from 1 to 5.

This index (D_i) is defined based on the attribute difference between the reference tree and its neighboring tree categories in the spatial structure unit. The difference index was obtained by counting the number of different attribute categories of trees in the spatial structure unit; the value of D_i ranges between 0 and 1.

Density (C): C_i was measured using Equation (3):

$$C_i = \frac{1}{4} \sum_{j=1}^4 Y_{ij} Y_{ij} = \begin{cases} 1, c > d \\ 0, c \leq d \end{cases} \quad (3)$$

where Y_{ij} is a discrete variable.

This index (C_i) was measured based on the crown and horizontal distance between the reference tree and the nearest neighboring trees. The exact definition is the comparison of the sum of the crown radius (c) and tree spacing (d). When $c > d$, crowns are overlapping, while $c \leq d$ means crowns are separate.

Angle index (W): Equation (4) was used for calculating W_i :

$$W_i = \frac{1}{4} \sum_{j=1}^4 Z_{ij} Z_{ij} = \begin{cases} 1, \alpha > \alpha_0 \\ 0, \alpha < \alpha_0 \end{cases} \quad (4)$$

where α is the angle between any two adjacent trees with the reference tree as the vertex and $\alpha_0 = 72^\circ$.

The angle index (W_i) calculates the ratio of the number of angle α greater than or equal to standard angle α_0 . It is used to determine the horizontal spatial distribution pattern of forest.

DBH size ratio (U): U_i was measured using Equation (5):

$$U_i = \frac{1}{4} \sum_{j=1}^4 K_{ij} K_{ij} = \begin{cases} 1, adjacent\ tree < reference\ tree \\ 0, adjacent\ tree > reference\ tree \end{cases} \quad (5)$$

where K_{ij} is a discrete variable, which is the number of reference trees with a DBH greater than that of adjacent trees.

The size ratio (U_i) reflects the degree of size difference between forests or other forest parameters. This is achieved by comparing the parameter size of the reference tree with surrounding trees of the same species as the reference tree. It was calculated as the proportion of adjacent trees that are smaller than the reference tree. Here, we specifically examined the DBH, height, and crown.

The height size ratio (H) is the same expression as the DBH size ratio.

Here, we selected as many reference trees as possible in each plot to maintain data accuracy. The mean of index ((MI) (Equation (6)) was calculated in each plot; then, the final SSP was calculated from the mean of six indices (Equation (7)).

$$MI = \frac{1}{n} \sum_{i=1}^n I_i \quad (6)$$

$$SSP = \frac{1}{6} \sum_{j=1}^6 MI_j \quad (7)$$

where n is the number of the reference trees in the plot and I is the value of the index in the unit where each reference tree is located; it can represent M, D, C, W, U, and H, respectively.

2.3. Field Measurements

On 2 July 2018, 52 sampling points were uniformly established in each of the four dump areas. The distribution of the sampling points is shown in Figure 2. A large plot (10 m × 10 m) was established for each sample point with four medium-sized plots (5 m × 5 m) established in each large plot, and a small plot (1 m × 1 m) established in each of the four medium-sized plots (Figure 2b). In total, 208 plots were established and investigated. We recorded the position of each large plot and measured the tree height, crown width, DBH, distance to adjacent trees, bush layer height, crown width and other indicators by using rulers, tape measures, and a Haglöf ECII electronic altimeter (Sweden).

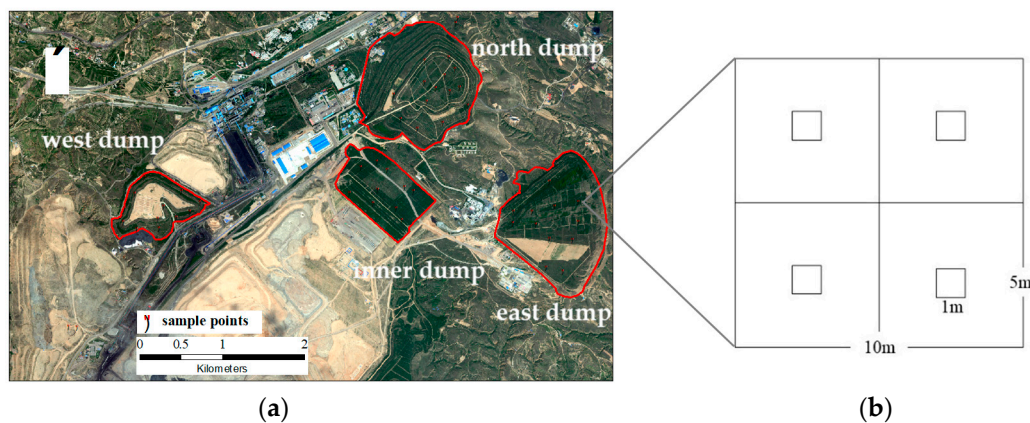


Figure 2. (a) Worldview-2 image showing the location of sampling points in Heidaigou open-pit coal mine; and (b) illustration of plot sampling strategy at each point.

2.4. Remote Sensing Data and Pre-Processing

The study used a Worldview-2 image with eight multispectral bands acquired on 30 June 2018. In addition to the four standard bands (blue, 450–510 nm; green, 510–580 nm; red, 630–690 nm; and near infrared, 770–895 nm), bands also included the coast (400–450 nm), yellow (585–625 nm), red edge (705–745 nm), and near-infrared 2 (860–1040 nm) bands. The data quality was good and the cloud volume was 0%. The image was pre-processed with geometric, radiation, and atmospheric correction as well as with image fusion. The panchromatic and multispectral bands of the Worldview-2 image were fused by the NDDifuse Pan Sharpening algorithm. The resolution of the image after fusion can reach 0.5 m, which can provide rich forest spectral and texture information.

2.5. Image Feature Extraction

Plant leaves have strong absorption characteristics in the visible red band and strong reflection characteristics in the near-infrared band [40], which causes different types of forest to have different degrees of spectral response [41,42]. Past research shows a vegetation index derived from a combination of different spectral bands has been widely used in the fields of forest type identification [43], physical parameter [44,45], and biochemical parameter [46,47] inversion. Fused Worldview-2 imagery can reach a resolution of 0.5 m, providing rich spectral and texture information. Therefore, this study extracted forest spectral and textural features in the images to construct a feature factor library of the forest spatial structure.

2.5.1. Construction of Feature Factor Library

The Worldview-2 satellite provides high-resolution remote sensing imagery containing eight-band spectral data. To estimate the SSPs of forest habitat, here we considered eight -band images using average values of each band. In addition, six vegetation indices were considered (Table 2): the Soil Adjusted Vegetation Index (SAVI), Ratio Vegetation Index (RVI), Enhanced Vegetation Index (EVI), Difference Vegetation Index (DVI), Normalized Difference Vegetation Index (NDVI), and Modified Soil Adjusted Vegetation Index (MSAVI).

Table 2. Selected six vegetation indices and their mathematical expressions.

Vegetation Index	Expression
Soil Adjusted Vegetation Index (SAVI)	$\frac{(1+L)(NIR-R)}{NIR+R+L}$
Ratio Vegetation Index (RVI)	NIR/R
Enhanced Vegetation Index (EVI)	$\frac{C_0 \times (NIR-R)}{NIR + C_1 \times NIR - C_2 \times B + C_3}$
Difference Vegetation Index (DVI)	$NIR - R$
Normalized Difference Vegetation Index (NDVI)	$(NIR - R) / (NIR + R)$
Modified Soil Adjusted Vegetation Index (MSAVI)	$\frac{(2NIR+1) - \sqrt{(2NIR+1)^2 - 8(NIR-R)}}{2}$

NIR, *R*, and *B* are near-infrared, red, and blue light bands, respectively. *L*, *C*₀, *C*₁, *C*₂, and *C*₃ are constants taking the values 0.5, 2.5, 6.0, 7.5, and 1, respectively.

Objects commonly have textural features on their surfaces; these are represented by the grey distribution of pixels and the surrounding spatial neighborhood of the object. The inherent characteristics of the object and its relationship with the surrounding environment cause obvious differences between the textural features of different objects. High spatial resolution optical images have rich textural features, which provide strong support for the extraction of textural features in the estimation of forest spatial structure.

Here, the second-order probability statistics filtering method was used to extract the textural features of typical forest and forest communities; multiple specification windows (3 × 3, 7 × 7, 9 × 9, 11 × 11, 13 × 13, 15 × 15, or 17 × 17 pixels) were selected for calculation. The eight-channel data of the Worldview-2 image participated in the calculation of the mean (*M*), variance (*V*), uniformity (*U*), contrast (*C*), dissimilarity (*D*), entropy (*E*), second-order angular moments (*S*), and correlation (*R*) of pixels in the image. The textural feature factor was composed of eight channels (eight spectral bands), seven windows (texture calculation windows), and eight texture parameters (band parameter calculation values) for a total of 448 measurements.

2.5.2. Screening of Feature Factor Library

The number of forest spectral and textural feature factors is very large in the primary feature factor library. In addition, many noise factors cause data redundancy. Therefore, correlation analysis [48] and random forest (RF) [49] were employed to select the dominant feature factors which make up the feature factor subset as the model input parameters.

Here, correlation analysis was carried out by SPSS to screen the feature factors for regression model. The feature factors for the mind evolutionary algorithm-back propagation (MEA-BP) neural network model was screened by the random forest variable importance scoring method. In the present study, a random forest variable importance scoring method was used to rank and filter the feature factor library. This algorithm was proposed by Breiman; the principle involves replacing the extracted samples from the original data to generate a new training sample set [49]. A classification tree is composed of the sample set from a random forest. The voting score of the classification tree was used to obtain the classification result. The random forest method has been widely used in various fields. It has the characteristics of high accuracy and good stability. In the processing of high-dimensional

arrays, random forest has a high tolerance for outliers giving it an importance score during array processing. Highly explanatory independent variable factors for dependent variables were filtered out based on this score. Here, we used out-of-bag data [50] as the optimal feature ordering condition; the optimal feature ordering of the spatial structure feature factors of the forest was performed.

2.6. Modeling

2.6.1. MEA-BP Neural Network Estimation Model

The MEA-BP neural network method is based on a back propagation network [51]. It adds “genetics,” “evolution,” “convergence,” and “alienation” to a multi-layer feedforward network based on an error back propagation operation. This algorithm can allow the avoiding of artificially defining the weight of each characteristic factor, thereby improving the reliability of the evaluation results. It can also inherit and popularize the winners’ existing empirical ideas [52].

Design of a forest spatial structure MEA-BP neural network

I Intermediate layer selection

Choosing the appropriate number of intermediate layers for the neural network can improve the prediction accuracy of the network and reduce the number of prediction errors. Here, a neural network structure with one intermediate layer was established based on the network convergence speed and data volume.

II Input layer nodes

According to the filtering result of the feature factor library, the number of input layer nodes was set to ten, and the specific input parameters were the parameter factors of the feature factor set after screening. One output layer was employed, which contains the SSPs to be extracted.

III Determination of the number of nodes in the hidden layer

The hidden layer nodes were determined according to an empirical formula, and the initial structural group was constructed using Equation (8):

$$h = \sqrt{n + m} + a \quad (8)$$

where h , n , and m are the number of nodes in the hidden, input, and output layers, respectively, and a is a constant in the range of [1,10]. The optimal number of nodes in the hidden layer was determined to be 12 by trial-and-error.

IV Activation function

Aiming at the three-layer network structure of this study, with one output layer, the Sigmoid function (Equation (9)) was selected as the intermediate layer activation function:

$$f(x) = \frac{1}{1 + e^{-x}} \quad (9)$$

V MEA parameter setting and data pre-processing

The initial population size was set to 200, and both the superior and temporary subpopulations were five. The normalized data were input into the model to reduce network errors.

2.6.2. Regression Estimation Model

Regression models are commonly used to estimate ecological parameters of forest habitats [53,54]. Because the forest SSPs are affected by multiple indicators, the following multiple regression model was introduced for parameter estimation. The optimal multivariate linear relationship expression between the spatial structure parameters and each characteristic factor was determined. The stability and accuracy of the regression model were verified using the sample test set in Equation (10):

$$y = ax_1 + bx_2 + cx_3 + \dots + zx_n \quad (10)$$

where y is the estimated value of the SSPs, x_i is the feature factor, and n is the number of the factors with high correlation with the SSPs.

2.7. Evaluation of Accuracy

Here, the coefficient of determination (R^2) and root mean square error (RMSE) were used to evaluate the accuracy of the model, as shown in Equations (11) and (12):

$$R^2 = 1 - \frac{\sum_{i=1}^n (\hat{y}_i - \bar{y})^2}{\sum_{i=1}^n (y_i - \bar{y})^2} \quad (11)$$

$$RMSE = \sqrt{\frac{1}{n} \sum_{i=1}^n (y_i - \hat{y}_i)^2} \quad (12)$$

where y_i and \hat{y}_i are the observations and predictions of the test set, respectively; \bar{y} is the average of the training set; and n is the number of training sets.

3. Results

3.1. Descriptive Statistics of Sample Points

The sampling points were divided into two groups, a group of 35 samples used as a training set and another set of 17 samples used as a test set. Basic statistical analysis of samples was carried out by computing the maximum, minimum, mean, standard deviation, and coefficient of variation (Table 3). The SSP range of the training set is 0.375–0.792 (mean = 0.538; standard deviation = 0.139). The SSP range of the test set is 0.333–0.750 (mean = 0.522; standard deviation = 0.136).

Table 3. Descriptive statistics of forest spatial structural parameters from 52 sampling points.

Data Set	N^1	Maximum	Minimum	Mean	Standard Deviation	Coefficient of Variation
Training set	35	0.792	0.375	0.538	0.139	0.258
Test set	17	0.750	0.333	0.522	0.136	0.260

¹ N is the number of samples.

3.2. The Feature Factors for Models

3.2.1. Feature Factors for Regression Model

The correlation analysis results show that textural features were the dominant parameters of the spatial structure of forest data (Table 4). Four feature factors were used in the selected feature factor set, among which three textural factors were all obtained by the 3×3 calculation window. As an exception, a significant positive correlation was observed between the mean value of spectral band 7 and the SSPs ($p \leq 0.001$); all other factors were significant ($p \leq 0.05$). The factor B7T3M (x_2) had the highest correlation with a correlation coefficient of 0.624. Note that the naming rule of textural feature factors (such as B7T3M) is: band number + texture calculation window + band parameters.

Table 4. Correlation between feature factors and spatial structural parameters.

Feature Factors	B8T3R (x_1)	B7T3M (x_2)	B5T3S (x_3)	NIR1 (x_4)
Correlation coefficient	0.535	0.624	0.567	0.540
Significance level	0.05	0.001	0.05	0.05

3.2.2. Feature Factors for MEA-BP Neural Network Model

Here, we have eight feature factor subsets. Among them, the Spvi only considers the spectral features which includes vegetation indices and image bands, while T3–T17 consider both spectral

features and textural features. T3, T7, T9, T11, T13, T15, and T17 represent the feature factors subsets obtained under 3×3 , 7×7 , 9×9 , 11×11 , 13×13 , 15×15 , and 17×17 calculation windows, respectively. Finally, ten feature factors were retained that make up the feature factor subset as the model input parameters.

In ordering the importance of the forest spatial structure feature factors, the textural feature factors occupy an absolute advantage in feature ranking (Table 5). The relevant textural parameters generated by image bands 3 and 6 are of high importance; these are mainly based on textural parameters such as dissimilarity, correlation, and variance. This coincides with the fact that each textural parameter is a feature describing the grey spatial distribution index.

Table 5. Feature factor subsets for mind evolutionary algorithm-back propagation neural network model.

Spvi	T3	T7	T9	T11	T13	T15	T17
NDVI	B3T3D	B3T7R	B3T9R	B3T11R	B3T13R	B3T15R	B3T17R
RVI	B6T3E	B6T7E	B5T9E	B5T11E	B6T13R	B6T15R	B2T17R
SAVI	RVI	B5T7E	B5T9C	B2T11R	B7T13V	B2T15R	B6T17R
MASVI	NDVI	B6T7R	B2T9V	B7T11V	B5T13V	B7T15H	B4T17R
EVI	SAVI	B5T7S	B5T9V	B5T11V	B7T13E	B5T15V	B7T17H
Blue	EVI	B5T7C	B2T9S	B6T11R	B4T13R	B4T15R	B7T17E
Coast blue	B3T3R	B5T7V	B6T9R	B2T11S	B7T13S	B6T15S	B7T17S
DVI	B6T3S	B2T7S	B5T9H	B8T11V	B5T13C	B7T15V	B7T17D
Nir2	B8T3E	B2T7E	B5T9E	B2T11V	B7T13D	B7T15E	B6T17E
Red	B8T3S	B5T7H	B2T9C	B7T11S	B5T13E	B6T15E	B5T17E

Naming rule of textural feature factors (such as B3T3D) is: band number + texture calculation window + band parameters; NDVI, normalized difference vegetation index; RVI, ratio vegetation index; SAVI, soil adjusted vegetation index; MASVI, modified soil adjusted vegetation index; EVI, enhanced vegetation index; DVI, difference vegetation index.

3.3. The Performance of Estimation

3.3.1. Regression Model

Correlation analysis shows that, among the feature factors, four SSPs had correlation coefficients greater than 0.5: B8T3R, B7T3M, B5T3S, and NIR1 (Table 4). It can be seen that the texture parameter was the main explanatory factor of the SSPs of the forests. Regression analysis of the relationship between the spatial structure parameters of forests and several optimal features:

$$y = 0.08x_1 - 0.008x_2 - 0.111x_3 - 0.19x_4 + 0.709$$

The model accuracy verification results are as follows: The model has an R value of 0.695, an R^2 of 0.553, a standard estimation error of 0.11452, an F value of 3.938, and $p < 0.005$ (Table 6). The $F(4,30)$ value is 2.69, which is less than 3.938, indicating that the model is statistically significant. Then, we applied a multiple linear regression model to the test set and obtained the relationship between the estimated and observed values (Figure 3). For this model, $R^2 = 0.6174$ and $RMSE = 0.1001$.

Table 6. The statistical parameters of variance analysis.

	Sum of Squares	df	Variance	F	p
Regression	0.206	4	0.058	3.938	0.011
Residual	0.214	30	0.015		
Sum	0.420	34			

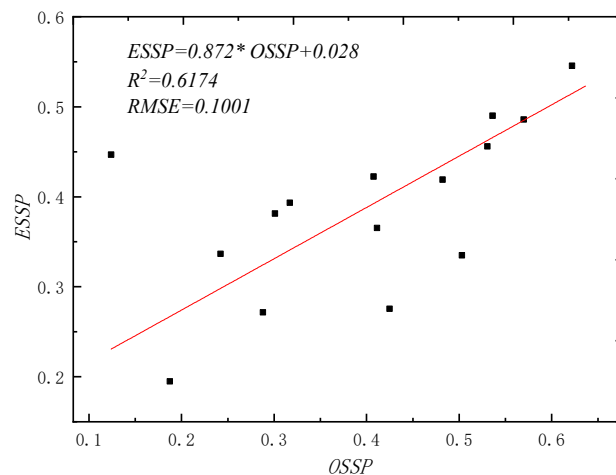


Figure 3. Relationship between the observed (OSSP) and estimated spatial structural parameters (ESSP) of restored forests in semi-arid mine dumps for validation analyses using a regression model (* represents multiplication).

3.3.2. MEA-BP Neural Network

The selected feature factor subsets were input into the MEA-BP neural network model to obtain the relationship between the observed values and the SSPs; the network values were subjected to inverse normalization to obtain the final estimates forest spatial structure. Table 7 summarizes the model accuracy of the estimation results of each feature factor subset. The results show that the estimation results of the forest SSP considering the image textural feature factor were significantly better than the simple spectral feature factor modeling. The feature factor subset of T3 had the highest accuracy and the strongest correlation was in each factor subset (Figure 4). The R^2 was highest (0.6975) and RMSE was smallest (0.0906).

Table 7. Accuracy of spatial structure parameter estimation with different feature factor subsets.

	Spvi	T3	T7	T9	T11	T13	T15	T17
R^2	-0.4679	0.6235	-0.0667	0.4621	0.2389	0.3972	0.4507	0.3913
RMSE	0.1461	0.0906	0.5265	0.1698	0.2140	0.1803	0.1452	0.1461

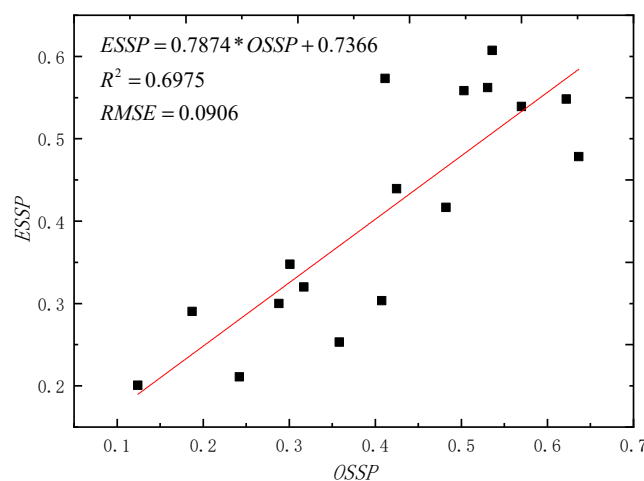


Figure 4. Relationship between simulated values and observed values of the mind evolutionary algorithm-back propagation neural network model based on the T3 feature factor subset. The T3 is a subset of textural feature factors based on the 3 × 3 calculation window. Note: observed (OSSP) and estimated spatial structural parameters (ESSP) (* represents multiplication).

3.4. Estimated Spatial Structure

The results of regression model and MEA-BP neural network show that the MEA-BP neural network method had a better inversion effect than the regression model method. The model calculated with the 3×3 texture window had the highest interpretability of the SSPs and was the most stable. We use an MEA-BP neural network model with a 3×3 texture windows to estimate forest SSPs. A trained neural network model was applied to the entire image. Each grey image was extracted as the model input object according to the optimal feature factor set. The network traverses the image and outputs the final forest SSP of each area of dumps (Figure 5).

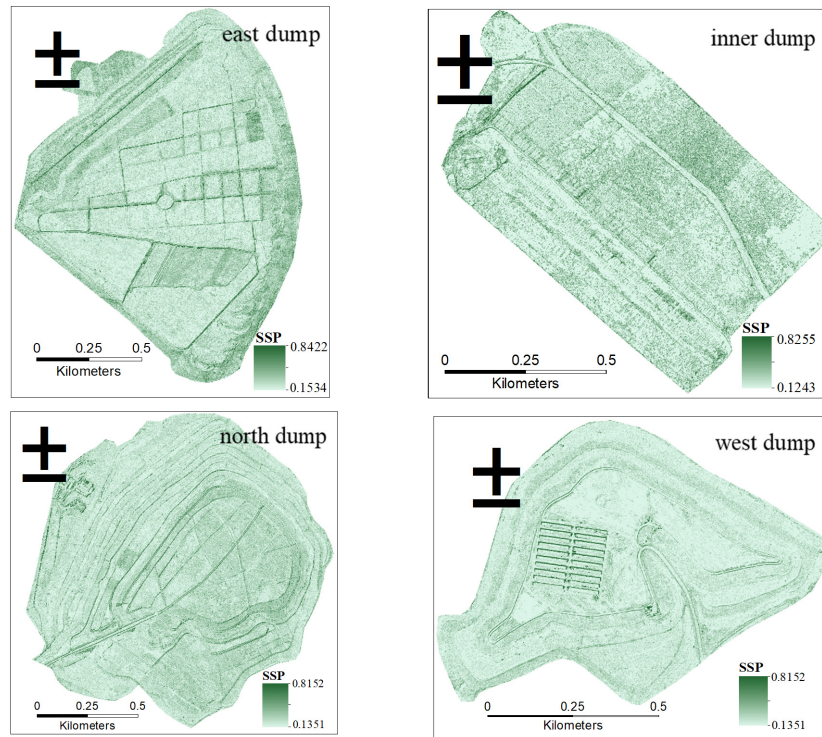


Figure 5. Spatial distribution of forest spatial structure in Heidaigou open-pit coal mine in the: east dump, inner dump, north dump, and west dump.

In vegetation restoration work, forest configuration types include tree (T), shrub (S), grass (G), tree–shrub (TS), tree–grass (TG), and tree–shrub–grass (TSG). The SSPs of each forest configuration type were calculated through the estimation results and land reclamation data of the mining area. Basic statistical analysis of different forest configuration types was carried out by computing the mean and difference (Table 8).

Table 8. Descriptive statistics of forest spatial structural parameters (SSPs) in different reclamation years from different forest configuration types.

SSP Year	Reclamation Years			Mean	Difference
	1995	2000	2008		
T	0.3453	0.4135	0.4366	0.39844	0.09133
S	0.3241	0.3654	0.3815	0.35702	0.05744
G	0.1484	0.1451	0.1531	0.14887	0.00470
TS	0.6398	0.7166	0.7265	0.69428	0.08670
TG	0.2541	0.2975	0.3315	0.29435	0.07740
TSG	0.6475	0.7632	0.7946	0.73509	0.14708
NR	0.1534	0.1721	0.1654	0.16363	0.01200

Forest configuration types: tree (T), shrub (S), grass (G), tree–shrub (TS), tree–grass (TG), and tree–shrub–grass (TSG).

The value ranges of the SSPs in the east, north, west, and inner areas of dumps were 0.1534–0.8422 (mean 0.4574), 0.1351–0.8152 (0.4670), 0.1351–0.8152 (0.4471), and 0.1243–0.8255 (0.4660), respectively (Figure 5). The greater spatial structure was found in the east dump, while the larger SSPs of the east dump were obviously larger than the other three areas of mine dumps. The images show that the forest SSPs were generally higher on the sides of roads and the edges of woodlands where most of the SSPs were greater than 0.7. The forest SSPs of the places where the forest configuration was TS and TSG were higher, generally between 0.60 and 0.85.

The results show that the spatial structural units with complex forest configuration and a high degree of mixing have higher SSPs. Forest SSPs have a certain indicative significance for the forest distribution status in the spatial structural unit. Therefore, the estimation of SSPs is more reliable based on Worldview-2 imagery using the MEA-BP neural network method.

4. Discussion

4.1. Variation of Spatial Structure

Here, we discuss the variability of the spatial structure of Heidaigou forests in combination with the forest planning data related to ecological restoration. The time nodes of the forest restoration timeline in the study area are 1995, 2000, and 2008. The SSPs of each forest configuration type were variable at different restoration years (Table 8).

Under the same restoration period, we sorted the six planted restoration configuration types according to the spatial structure parameters finding that: TSG > TS > T > S > TG > Native Remnant (NR) > G (Figure 6a). The estimation results show that the spatial structure stability of the TSG type was the highest, averaging 0.7351, while the SSP of the grass was 0.1489 with a spatial structure stability lower than that of native remnant (average 0.1636). The results indicate that diverse types of forest configuration are more conducive to the renewal, increase biodiversity, and enhance self-enrichment of forests.

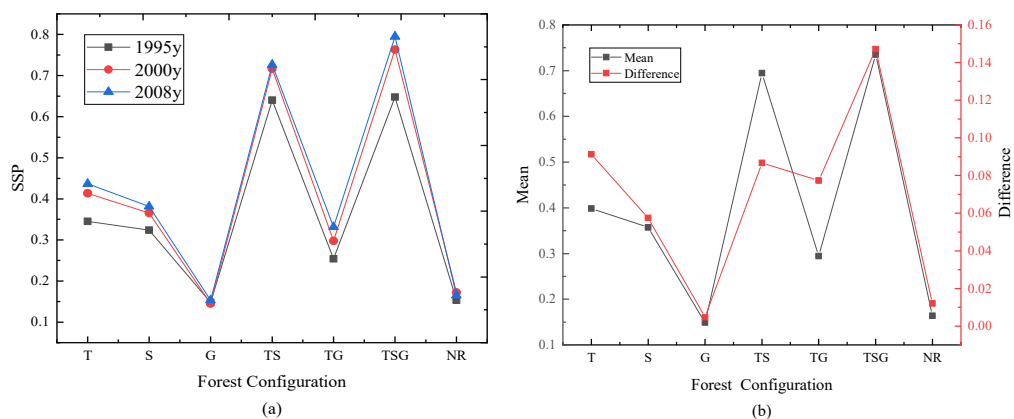


Figure 6. (a) Spatial structural parameters (SSP) of each forest configuration type at different restoration years, and (b) evaluation of forest spatial structure variability by means and differences. Note: T, tree; S, shrub; G, grass; TS, tree–shrub; TG, tree–grass; TSG, tree–shrub–grass.

Under the same forest configuration type, the spatial structure of other forest configuration types showed 1995 < 2000 < 2008 while the performance of simple grass structure was 2000 < 1995 < 2008. In addition, the spatial structure parameters of each forest configuration type showed an increasing trend with extending restoration time, which increased by 0.0913 (T), 0.0574 (S), 0.0047 (G), 0.0867 (TS), 0.0774 (TG), and 0.1471 (TSG). The TSG and G types had the largest and smallest growth rates, respectively (Figure 6b). These results indicate that the overall spatial structure stability of the forest community in the study area increased over time after restoration, and is generally superior to that of the native remnant. This indicates that the semi-arid planted and restored forest has shown renewed vigor.

4.2. Limitations and Future Work

The restored forest in semi-arid mine dumps study area has a sparse structure, so the textural features are significantly different from other areas, which allows the textural feature factors to be well-extracted. Additionally, the restored forest was planted and reconstructed based on a restoration plan, which created a regular distribution pattern of forest trees. The regular distribution makes the textural features separable through 3×3 calculation windows. Therefore, the estimation of forest SSPs can be achieved in this area of semi-arid mine dumps. However, the feasibility of this method in other areas still needs to be tested. For example, tropical forests feature a complex space structures [55], and the SSPs cannot be reflected using only optical imagery. The estimation results of the forest SSPs using the random forest had an accuracy of only 0.6975, which was affected by the non-forest land cover such as roads in the area of mine dumps. Future research could try to mask the image to improve the visual effects. Data related to only one scene image were available for each year in the present study due to the limitations of time and data. In fact, the SSPs change over time. Therefore, a complete evaluation of the SSPs will require multiple periods of data.

Currently, scholars use laser light detection and ranging (LiDAR) technology to extract the three-dimensional structure of forests [56,57]. Many parameters can be obtained using LiDAR, such as canopy height [58], leaf area distribution [59], leaf area profile [60], and stem size distribution [61]. The laser pulse emitted by the LiDAR can penetrate the forest canopy to obtain the three-dimensional structure information of forests. Its data are presented in the form of a point cloud. Each discrete point cloud contains three-dimensional coordinate value and intensity value information. However, it does not have the spectral and texture information that Worldview-2 images can provide. In the future, researchers can integrate image and LiDAR [62] data sources to estimate the forest spatial structure to improve accuracy, but the cost of LiDAR needs to be considered. For example, unmanned aerial vehicle equipped with LiDAR [63–65] can conduct large-scale ecological evaluation but the cost is higher. Usually, it is difficult for the closed mines to provide funding to support ecological assessments. All of the above situations require the techniques to save costs. In addition, future research can focus on identifying the core driving force of the changes in the forest SSPs by combining a restoration plan with other forest biochemical parameters. Furthermore, a method for estimating the spatial structure of forests can be developed.

5. Conclusions

In this study, the MEA-BP neural network model was established to estimate the restored forest SSP based on Worldview-2 imagery. The random forest method was used to screen out the feature factors with high explanatory ability to the SSP. Textural feature factors were found to be more closely correlated with spatial structure than spectral feature factors. High spatial resolution Worldview-2 satellite imagery is feasible for use in parameter estimation of forest spatial structure. In addition, under different forest configuration modes in different restoration years, the spatial structure of forests varies. Therefore, forest spatial structure should be considered as an indicator when evaluating ecological restoration efforts.

In the future, different continuous time-series datasets could be integrated for further experiments. Through the use of these data, the accuracy of the MEA-BP neural network modeling can be improved, and dynamic vegetation monitoring in mined areas can be realized. In addition, the correlation between the spatial structure parameters and other forest parameters can also be studied, which provides theoretical support for decision-making-based adjustment of ecological restoration management related to forest configuration.

Author Contributions: X.Z. conceived and designed the study; X.Z., Y.Z., Y.Y., H.H., S.Z., and R.L. were involved in data preparation, X.Z., Y.Y., and H.H. processed the data, Y.Z., Y.Y., and R.L. were involved in field work, X.Z. analyzed the data, X.Z., Y.Z., Y.Y., and H.H. validated the results, X.Z. prepared maps and figures; and X.Z. wrote the paper with the help of all co-authors. All authors have read and agreed to the published version of the manuscript.

Funding: This work was supported by the Fundamental Research Funds for the Central Universities under Grant No. 2017XKZD14.

Acknowledgments: We would like to thank Shenhua Zhungeer Energy Co. Ltd. for supporting fieldwork.

Conflicts of Interest: The authors declare no conflict of interest.

References

1. Yang, Y.; Erskine, P.D.; Lechner, A.M.; Mulligan, D.; Zhang, S.; Wang, Z. Detecting the dynamics of vegetation disturbance and recovery in surface mining area via Landsat imagery and LandTrendr algorithm. *J. Clean. Prod.* **2018**, *178*, 353–362. [\[CrossRef\]](#)
2. Iizuka, K.; Yonehara, T.; Itoh, M.; Kosugi, Y. Estimating Tree Height and Diameter at Breast Height (DBH) from Digital Surface Models and Orthophotos Obtained with an Unmanned Aerial System for a Japanese Cypress (*Chamaecyparis obtusa*) Forest. *Remote Sens.* **2018**, *10*, 13. [\[CrossRef\]](#)
3. Randlane, T.; Tullus, T.; Saag, A.; Lutter, R.; Tullus, A.; Helm, A.; Tullus, H.; Partel, M. Diversity of lichens and bryophytes in hybrid aspen plantations in Estonia depends on landscape structure. *Can. J. For. Res.* **2017**, *47*, 1202–1214. [\[CrossRef\]](#)
4. Wernsdorfer, H.; Colin, A.; Bontemps, J.D.; Chevalier, H.; Pignard, G.; Cauria, S.; Leban, J.M.; Herve, J.C.; Fournier, M. Large-scale dynamics of a heterogeneous forest resource are driven jointly by geographically varying growth conditions, tree species composition and stand structure. *Ann. Sci.* **2012**, *69*, 829–844. [\[CrossRef\]](#)
5. Dong, L.; Wei, H.; Liu, Z. Optimizing Forest Spatial Structure with Neighborhood-Based Indices: Four Case Studies from Northeast China. *Forests* **2020**, *11*, 413. [\[CrossRef\]](#)
6. Bergseng, E.; Ask, J.A.; Framstad, E.; Gobakken, T.; Solberg, B.; Hoen, H.F. Biodiversity protection and economics in long term boreal forest management—A detailed case for the valuation of protection measures. *For. Policy Econ.* **2012**, *15*, 12–21. [\[CrossRef\]](#)
7. Ozdemir, I.; Karnieli, A. Predicting forest structural parameters using the image texture derived from Worldview-2 multispectral imagery in a dryland forest, Israel. *Int. J. Appl. Earth Obs. Geoinf.* **2011**, *13*, 701–710. [\[CrossRef\]](#)
8. Mitchell, M.G.E.; Wu, D.; Johansen, K.; Maron, M.; McAlpine, C.; Rhodes, J.R.; Lee, T.M. Landscape structure influences urban vegetation vertical structure. *J. Appl. Ecol.* **2016**, *53*, 1477–1488. [\[CrossRef\]](#)
9. Leempoel, K.; Bourgeois, C.; Zhang, J.; Wang, J.; Dahdouh-Guebas, F.; Bogaert, J. Spatial heterogeneity in the mangrove vegetation structure in the Zhanjiang Mangrove National Nature Reserve (China): An approach using remote sensing (GeoEye-1 imagery) and GIS-analysis. *VLIZ Spec. Publ.* **2012**, *43*, 68–76.
10. Ferreira, J.N.; Bustamante, M.; Garcia-Montiel, D.C.; Caylor, K.K.; Davidson, E.A. Spatial variation in vegetation structure coupled to plant available water determined by two-dimensional soil resistivity profiling in a Brazilian savanna. *Oecologia* **2007**, *153*, 417–430. [\[CrossRef\]](#)
11. Claverie, M.; Demarez, V.; Duchemin, B.; Hagolle, O.; Ducrot, D.; Marais-Sicre, C.; Dejoux, J.-F.; Huc, M.; Keravec, P.; Béziat, P.; et al. Maize and sunflower biomass estimation in southwest France using high spatial and temporal resolution remote sensing data. *Remote Sens. Environ.* **2012**, *124*, 844–857. [\[CrossRef\]](#)
12. White, J.C.; Coops, N.C.; Wulder, M.A.; Vastaranta, M.; Hilker, T.; Tompalski, P. Remote Sensing Technologies for Enhancing Forest Inventories: A Review. *Can. J. Remote Sens.* **2016**, *42*, 619–641. [\[CrossRef\]](#)
13. Bao, N.; Lechner, A.M.; Johansen, K.; Ye, B. Object-based classification of semi-arid vegetation to support mine rehabilitation and monitoring. *J. Appl. Remote Sens.* **2014**, *8*. [\[CrossRef\]](#)
14. Luhar, M.; Rominger, J.; Nepf, H. Interaction between flow, transport and vegetation spatial structure. *Environ. Fluid Mech.* **2008**, *8*, 423–439. [\[CrossRef\]](#)
15. Mohseni, N.; Sepehr, A.; Hosseinzadeh, S.R.; Golzarian, M.R.; Shabani, F. Variations in spatial patterns of soil-vegetation properties over subsidence-related ground fissures at an arid ecotone in northeastern Iran. *Environ. Earth Sci.* **2017**, *76*, 13. [\[CrossRef\]](#)
16. Diouf, A.; Barbier, N.; Mahamane, A.; Lejoly, J.; Saadou, M.; Bogaert, J. Characterization of the spatial structure of woody species in “gapped bush” vegetation in southwest Niger. *Can. J. For. Res.* **2010**, *12*, 1201–1220. [\[CrossRef\]](#)
17. Muchoney, D.; Strahler, A. Regional vegetation mapping and direct land surface parameterization from remotely sensed and site data. *Int. J. Remote Sens.* **2002**, *23*, 1125–1142. [\[CrossRef\]](#)

18. Mallinis, G.; Mitsopoulos, I.; Chrysafi, I. Evaluating and comparing Sentinel 2A and Landsat-8 Operational Land Imager (OLI) spectral indices for estimating fire severity in a Mediterranean pine ecosystem of Greece. *GiScience Remote Sens.* **2017**, *55*, 1–18. [[CrossRef](#)]
19. Kazar, S.A.; Warner, T.A. Assessment of carbon storage and biomass on minelands reclaimed to grassland environments using Landsat spectral indices. *J. Appl. Remote Sens.* **2013**, *7*. [[CrossRef](#)]
20. Zhang, C.; Ren, H.; Huang, Z.; Li, J.; Qin, Q.; Zhang, T.; Sun, Y. Assessment of the application of copper stress vegetation index on Hyperion image in Dexing Copper Mine, China. *J. Appl. Remote Sens.* **2019**, *13*. [[CrossRef](#)]
21. Phillip, M.K.; Stuart, P.; Peter, E. Fire Severity and Vegetation Recovery on Mine Site Rehabilitation Using Worldview-3 Imagery. *Fire* **2018**, *1*, 22.
22. Mateo-Sanchis, A.; Munoz-Mari, J.; Perez-Suay, A.; Camps-Valls, G. Warped Gaussian Processes in Remote Sensing Parameter Estimation and Causal Inference. *IEEE Geosci. Remote Sens. Lett.* **2018**, *15*, 1647–1651. [[CrossRef](#)]
23. Mettas, C.; Agapiou, A.; Themistocleous, K.; Neocleous, K.; Hadjimitsis, D.G. Detection of asphalt pavement cracks using remote sensing techniques. In Proceedings of the Remote Sensing Technologies And Applications In Urban Environments, Edinburgh, UK, 26–27 September 2016; Erbertseder, T., Esch, T., Chrysoulakis, N., Eds.; SPIE: Bellingham, WA, USA, 2016; Volume 10008.
24. Zeng, X.; Liu, Z.; He, C.; Ma, Q.; Wu, J. Detecting surface coal mining areas from remote sensing imagery: An approach based on object-oriented decision trees. *J. Appl. Remote Sens.* **2017**, *11*. [[CrossRef](#)]
25. Kaplan, G.; Avdan, U. Monthly Analysis of Wetlands Dynamics Using Remote Sensing Data. *ISPRS Int. J. Geo-Inf.* **2018**, *7*, 411. [[CrossRef](#)]
26. Gasparovic, M.; Rumora, L.; Miler, M.; Medak, D. Effect of fusing Sentinel-2 and Worldview-4 imagery on the various vegetation indices. *J. Appl. Remote Sens.* **2019**, *13*. [[CrossRef](#)]
27. Kayet, N.; Pathak, K.; Chakrabarty, A.; Sahoo, S. Urban heat island explored by co-relationship between land surface temperature vs multiple vegetation indices. *Spat. Inf. Res.* **2016**, *24*, 515–529. [[CrossRef](#)]
28. Kiala, Z.; Odindi, J.; Mutanga, O.; Peerbhay, K. Comparison of partial least squares and support vector regressions for predicting leaf area index on a tropical grassland using hyperspectral data. *J. Appl. Remote Sens.* **2016**, *10*. [[CrossRef](#)]
29. Mutowo, G.; Mutanga, O.; Masocha, M. Mapping foliar N in miombo woodlands using sentinel-2 derived chlorophyll and structural indices. *J. Appl. Remote Sens.* **2018**, *12*. [[CrossRef](#)]
30. Kozoderov, V.V.; Dmitriev, E.V.; Melnik, P.G.; Donskoi, S.A. Evaluation of the Species Composition and the Biological Productivity of Forests Based on Remote Sensing Data with High Spatial and Spectral Resolution. *Izv. Atmos. Ocean. Phys.* **2018**, *54*, 1374–1380. [[CrossRef](#)]
31. DeTar, W.R.; Penner, J.V. Airborne remote sensing used to estimate percent canopy cover and to extract canopy temperature from scene temperature in cotton. *Trans. Asabe* **2007**, *50*, 495–506. [[CrossRef](#)]
32. Grosse-Stoltenberg, A.; Hellmann, C.; Werner, C.; Oldeland, J.; Thiele, J. Evaluation of Continuous VNIR-SWIR Spectra versus Narrowband Hyperspectral Indices to Discriminate the Invasive *Acacia longifolia* within a Mediterranean Dune Ecosystem. *Remote Sens.* **2016**, *8*, 334. [[CrossRef](#)]
33. Wang, Z.; Lechner, A.M.; Yang, Y.; Baumgartl, T.; Wu, J. Mapping the cumulative impacts of long-term mining disturbance and progressive rehabilitation on ecosystem services. *Sci. Total Environ.* **2020**, *717*, 137214. [[CrossRef](#)] [[PubMed](#)]
34. Zhang, M.; Wang, J.; Feng, Y. Temporal and spatial change of land use in a large-scale opencast coal mine area: A complex network approach. *Land Use Policy* **2019**, *86*, 375–386. [[CrossRef](#)]
35. Elhag, M.; Gitas, I.; Othman, A.; Bahrawi, J.; Gikas, P. Assessment of Water Quality Parameters Using Temporal Remote Sensing Spectral Reflectance in Arid Environments, Saudi Arabia. *Water* **2019**, *11*, 556. [[CrossRef](#)]
36. Lausch, A.; Pause, M.; Merbach, I.; Gwilym-Margianto, S.; Schulz, K.; Zacharias, S.; Seppelt, R. Scale-specific Hyperspectral Remote Sensing Approach in Environmental Research. *Photogramm. Fernerkund. Geoinf.* **2012**, 589–601. [[CrossRef](#)]
37. Weissteiner, C.J.; Strobl, P.; Sommer, S. Assessment of status and trends of olive farming intensity in EU-Mediterranean countries using remote sensing time series and land cover data. *Ecol. Indic.* **2011**, *11*, 601–610. [[CrossRef](#)]

38. Zhan, Y.; Su, Y.; Huang, J.; Ye, F.; Zhang, C. Mineral recognition mapping using measured spectra based on classification and regression tree. *J. Appl. Remote Sens.* **2016**, *10*. [[CrossRef](#)]
39. Zhou, C.; Wang, B.; Wang, W.; Zhao, P.; Li, W. Stability evaluation of different forest communities in Huanglongshan mountain based on the spatial structure index. *J. Cent. South Univ. For. Technol.* **2018**, *38*, 76–82. [[CrossRef](#)]
40. Verrelst, J.; Rivera, J.P.; Gitelson, A.; Delegido, J.; Moreno, J.; Camps-Valls, G. Spectral band selection for vegetation properties retrieval using Gaussian processes regression. *Int. J. Appl. Earth Obs. Geoinf.* **2016**, *52*, 554–567. [[CrossRef](#)]
41. Dandois, J.P.; Ellis, E.C. High spatial resolution three-dimensional mapping of vegetation spectral dynamics using computer vision. *Remote Sens. Environ.* **2013**, *136*, 259–276. [[CrossRef](#)]
42. Keshava, N.; Mustard, J.F. Spectral unmixing. *IEEE Signal Process. Mag.* **2002**, *19*, 44–57. [[CrossRef](#)]
43. Schmidt, K.S.; Skidmore, A.K. Spectral discrimination of vegetation types in a coastal wetland. *Remote Sens. Environ.* **2003**, *85*, 92–108. [[CrossRef](#)]
44. Verrelst, J.; Rivera, J.P.; Leonenko, G.; Alonso, L.; Moreno, J. Optimizing LUT-Based RTM Inversion for Semiautomatic Mapping of Crop Biophysical Parameters from Sentinel-2 and-3 Data: Role of Cost Functions. *IEEE Trans. Geosci. Remote Sens.* **2014**, *52*, 257–269. [[CrossRef](#)]
45. Wallace, A.; Nichol, C.; Woodhouse, I. Recovery of Forest Canopy Parameters by Inversion of Multispectral LiDAR Data. *Remote Sens.* **2012**, *4*, 509–531. [[CrossRef](#)]
46. Mutanga, O.; Adam, E.; Cho, M.A. High density biomass estimation for wetland vegetation using Worldview-2 imagery and random forest regression algorithm. *Int. J. Appl. Earth Obs. Geoinf.* **2012**, *18*, 399–406. [[CrossRef](#)]
47. Vastaranta, M.; Yu, X.; Luoma, V.; Karjalainen, M.; Saarinen, N.; Wulder, M.A.; White, J.C.; Persson, H.J.; Hollaus, M.; Yrttimaa, T.; et al. Aboveground forest biomass derived using multiple dates of Worldview-2 stereo-imagery: Quantifying the improvement in estimation accuracy. *Int. J. Remote Sens.* **2018**, *39*, 8766–8783. [[CrossRef](#)]
48. Yakimov, V.N. General problems of metrology and measurement technique—The structural design of digital correlometers for operational correlation analysis based on sign-function analog-stochastic quantization. *Meas. Tech.* **2007**, *50*, 356–363. [[CrossRef](#)]
49. Breiman, L. Random Forests. *Mach. Learn.* **2001**, *45*, 5–32. [[CrossRef](#)]
50. Zhang, Y.Q.; Cao, G.; Li, X.S.; Wang, B.S. Cascaded Random Forest for Hyperspectral Image Classification. *IEEE J. Sel. Top. Appl. Earth Obs. Remote Sens.* **2018**, *11*, 1082–1094. [[CrossRef](#)]
51. Maren, A.; Jones, D.; Franklin, S. Configuring and optimizing the back-propagation network. In *Handbook of Neural Computing Applications*; Elsevier: Amsterdam, The Netherlands, 1990; pp. 237–250. [[CrossRef](#)]
52. Wang, W.; Tang, R.; Li, C.; Liu, P.; Luo, L. A BP neural network model optimized by Mind Evolutionary Algorithm for predicting the ocean wave heights. *Ocean Eng.* **2018**, *162*, 98–107. [[CrossRef](#)]
53. Jagodziński, A.M.; Zasada, M.; Bronisz, K.; Bronisz, A.; Bijak, S. Biomass conversion and expansion factors for a chronosequence of young naturally regenerated silver birch (*Betula pendula* Roth) stands growing on post-agricultural sites. *For. Ecol. Manag.* **2017**, *384*, 208–220. [[CrossRef](#)]
54. Wing, B.M.; Ritchie, M.W.; Boston, K.; Cohen, W.B.; Gitelman, A.; Olsen, M.J. Prediction of understory vegetation cover with airborne lidar in an interior ponderosa pine forest. *Remote Sens. Environ.* **2012**, *124*, 730–741. [[CrossRef](#)]
55. John, R.; Dalling, J.W.; Harms, K.E.; Yavitt, J.B.; Stallard, R.F.; Mirabello, M.; Hubbell, S.P.; Valencia, R.; Navarrete, H.; Vallejo, M.; et al. Soil nutrients influence spatial distributions of tropical tree species. *Proc. Natl. Acad. Sci. USA* **2007**, *104*, 864–869. [[CrossRef](#)] [[PubMed](#)]
56. Caynes, R.J.C.; Mitchell, M.G.E.; Wu, D.S.; Johansen, K.; Rhodes, J.R. Using high-resolution LiDAR data to quantify the three-dimensional structure of vegetation in urban green space. *Urban Ecosyst.* **2016**, *19*, 1749–1765. [[CrossRef](#)]
57. Owers, C.J.; Rogers, K.; Woodroffe, C.D. Identifying spatial variability and complexity in wetland vegetation using an object-based approach. *Int. J. Remote Sens.* **2016**, *37*, 4296–4316. [[CrossRef](#)]
58. Lim, K.; Treitz, P.; Wulder, M.; St-Onge, B.; Flood, M. LiDAR remote sensing of forest structure. *Prog. Phys. Geogr.* **2003**, *27*, 88–106. [[CrossRef](#)]
59. Béland, M.; Baldocchi, D.D.; Widlowski, J.-L.; Fournier, R.A.; Verstraete, M.M. On seeing the wood from the leaves and the role of voxel size in determining leaf area distribution of forests with terrestrial LiDAR. *Agric. For. Meteorol.* **2014**, *184*, 82–97. [[CrossRef](#)]

60. Choi, H.; Song, Y.; Jang, Y. Urban Forest Growth and Gap Dynamics Detected by Yearly Repeated Airborne Light Detection and Ranging (LiDAR): A Case Study of Cheonan, South Korea. *Remote Sens.* **2019**, *11*, 1551. [[CrossRef](#)]
61. Mulverhill, C.; Coops, N.C.; White, J.C.; Tompalski, P.; Marshall, P.L. Structural development following stand-replacing disturbance in a boreal mixedwood forest. *For. Ecol. Manag.* **2019**, *453*. [[CrossRef](#)]
62. Szostak, M.; Pietrzykowski, M.; Likus-Cieslik, J. Reclaimed Area Land Cover Mapping Using Sentinel-2 Imagery and LiDAR Point Clouds. *Remote Sens.* **2020**, *12*, 261. [[CrossRef](#)]
63. Koska, B.; Jirka, V.; Urban, R.; Kremen, T.; Hesslerov, P.; Jon, J.; Pospisil, J.; Fogl, M. Suitability, characteristics, and comparison of an airship UAV with lidar for middle size area mapping. *Int. J. Remote Sens.* **2017**, *38*, 2973–2990. [[CrossRef](#)]
64. Urban, R.; Koska, B.; Moudry, V.; Solsky, M.; Sgem. Terrain of Post Mining Site from Airship Lidar. In Proceedings of the Informatics, Geoinformatics And Remote Sensing Conference Proceedings, Sgem 2016, Vol II, Albena, Bulgaria, 30 June–6 July 2016; pp. 577–584.
65. Ostrowski, W.; Górski, K.; Pilarska, M.; Salach, A.; Bakuła, K. Comparison of the laser scanning solutions for the unmanned aerial vehicles. *Arch. Photogramm. Cart. Remote Sens.* **2017**, *29*, 101–123. [[CrossRef](#)]



© 2020 by the authors. Licensee MDPI, Basel, Switzerland. This article is an open access article distributed under the terms and conditions of the Creative Commons Attribution (CC BY) license (<http://creativecommons.org/licenses/by/4.0/>).